01 Jan 2023

Boro/carbothermal Reduction Co-Synthesis of Dual-Phase High-Entropy Boride-Carbide Ceramics

Lun Feng

William Fahrenholtz
Missouri University of Science and Technology, billf@mst.edu

Gregory E. Hilmas

Stefano Curtarolo

Recommended Citation

L. Feng et al., "Boro/carbothermal Reduction Co-Synthesis of Dual-Phase High-Entropy Boride-Carbide Ceramics," *Journal of the European Ceramic Society*, Elsevier, Jan 2023.
The definitive version is available at https://doi.org/10.1016/j.jeurceramsoc.2022.12.056

Journal of the European Ceramic Society 43 (2023) 2708–2712

Contents lists available at ScienceDirect

Journal of the European Ceramic Society

journal homepage: www.elsevier.com/locate/jeurceramsoc

Short communication

Boro/carbothermal reduction co-synthesis of dual-phase high-entropy boride-carbide ceramics

Lun Feng [a,*], William G. Fahrenholtz [a], Gregory E. Hilmas [a], Stefano Curtarolo [b,c]

[a] Department of Materials Science and Engineering, Missouri University of Science and Technology, Rolla, MO 65049, USA
[b] Department of Mechanical Engineering and Materials Science, Duke University, Durham, NC 27708, USA
[c] Center for Autonomous Materials Design, Duke University, Durham, NC 27708, USA

ARTICLE INFO

Keywords:
Ultra-high temperature ceramics
High-entropy boride
High-entropy carbide
Microstructure
Vickers hardness

ABSTRACT

Dense, dual-phase (Cr,Hf,Nb,Ta,Ti,Zr)B_2-(Cr,Hf,Nb,Ta,Ti,Zr)C ceramics were synthesized by boro/carbothermal reduction of oxides and densified by spark plasma sintering. The high-entropy carbide content was about 14.5 wt %. Grain growth was suppressed by the pinning effect of the two-phase ceramic, which resulted in average grain sizes of 2.7 ± 1.3 μm for the high-entropy boride phase and 1.6 ± 0.7 μm for the high-entropy carbide phase. Vickers hardness values increased from 25.2 ± 1.1 GPa for an indentation load of 9.81 N to 38.9 ± 2.5 GPa for an indentation load of 0.49 N due to the indentation size effect. Boro/carbothermal reduction is a facile process for the synthesis and densification of dual-phase high entropy boride-carbide ceramics with both different combinations of transition metals and different proportions of boride and carbide phases.

1. Introduction

High-entropy ultra-high-temperature boride (HEB) and carbide (HEC) ceramics have received attention for their potential applications in extreme environments due to their improved elevated temperature mechanical properties, thermal stability, and oxidation resistance compared to individual transition metal borides and carbides [1–6]. A previous study on the effect of compositions on the Vickers hardness of high-entropy diboride ceramics found that $(Cr_{0.2}Hf_{0.2}Ta_{0.2}Ti_{0.2}Zr_{0.2})B_2$ (48.3 ± 2.3 GPa at a load of 0.49 N) and $(Hf_{0.2}Ta_{0.2}Ti_{0.2}W_{0.2}Zr_{0.2})B_2$, (45.8 ± 5.3 GPa at a load of 0.49 N) had the highest Vickers hardness values among the reported compositions[7]. Another study indicated that $(Hf_{0.2}Nb_{0.2}Ta_{0.2}Ti_{0.2}Zr_{0.2})C$ ceramics had a Vickers hardness of 28.7 ± 0.6 GPa at a load of 1.96 N, which was higher than those reported in previous studies of the same composition [8–10]. In addition, $(Hf_{0.2}Nb_{0.2}Ta_{0.2}Ti_{0.2}Zr_{0.2})C$ ceramics exhibited better flexural strength retention up to 1800°C than the individual carbides [3].

Several studies of dual-phase HEB-HEC ceramics have been reported to date. Qin et al. [11] produced a series of dual-phase HEB-HEC ceramics with different ratios of (Hf,Nb,Ta,Ti,Zr)B_2 and (Hf,Nb,Ta,Ti,Zr)C by spark plasma sintering (SPS) of commercial transition metal boride and carbide powders that were mixed by high energy ball milling. The effects of compositions on the grain size, mechanical properties, and thermal conductivities of dual-phase HEB-HEC ceramics were investigated. However, due to the application of high-energy ball milling and commercial powders, tungsten and oxygen impurities were introduced, which resulted in low relative densities of 92.4%. Similarly, Huo et al. [12] produced dual-phase HEB-HEC ceramics by reactive hot pressing (RHP) of TiC and commercial diboride powders according to the reaction: $TMB_2 + TiC \rightarrow TiB_2 + TMC$ where TM is an abbreviation of transition metals. The resulting ceramic had a Vickers hardness of 28.4 ± 1.5 GPa at 9.8 N, flexural strength of 1017 ± 91 MPa, and fracture toughness 4.7 ± 0.3 MPa·$m^{1/2}$. In contrast, to minimize the contamination and promote the densification, Luo et al. [13] synthesized dual-phase (Hf,Nb,Ta,Ti,Zr)B_2-(Hf,Nb,Ta,Ti,Zr)C ceramics with different boride-to-carbide ratios by SPS of powder mixtures synthesized via boro/carbothermal reduction (BCTR) reaction. As-synthesized powder mixtures had fine particle size, promoting the densification and fine microstructure of final ceramics. A previous study [14] reported a two-step process for the synthesis of (Hf,Nb,Ta,Ti,Zr)C-(Hf,Nb,Ta,Ti,Zr)B_2 ceramics. Firstly, (Hf,Nb,Ta,Ti,Zr)C was synthesized by carbothermal reduction of oxides. Then, (Hf,Nb,Ta,Ti,Zr)C was partially converted to $(HfNbTaTiZr)B_2$ by reacting the HEC with B_4C and ZrH_2. These previous studies used high-energy ball milling to reduce the particle size of starting powders and promote densification, which introduces impurities that affect the final composition and properties. For example, oxide impurities can

* Corresponding author.
E-mail address: allen13521@gmail.com (L. Feng).

https://doi.org/10.1016/j.jeurceramsoc.2022.12.056
Received 21 September 2022; Received in revised form 19 December 2022; Accepted 21 December 2022
Available online 22 December 2022

decrease both strength and hardness.

The purpose of the present study was to investigate the synthesis and densification of dual-phase HEB-HEC ceramics without introducing detrimental impurities.

2. Experimental procedure

Chromium oxide (Cr_2O_3, 99.5%, 0.7 μm, Elementis, Corpus Christi, TX), hafnium oxide (HfO_2, 99%, −325 mesh, Alfa Aesar, Tewksbury, MA), niobium oxide (Nb_2O_5, 99.5%, −100 mesh, Alfa Aesar), titanium oxide (TiO_2, 99.9%, 32 nm APS, Alfa Aesar, Tewksbury, MA), zirconium oxide (ZrO_2, 99%, 5 μm, Sigma-Aldrich, St. Louis, MO), tantalum oxide (Ta_2O_5, 99.8%, 1–5 μm, Atlantic Equipment Engineers, Upper Saddle River, NJ), boron carbide (B_4C, purity 96.8%, 0.3–0.6 μm, HD-20, H.C. Starck, Karlsruhe, Germany) and carbon black (C, BP1100, Cabot, Alpharetta, GA) were used as the starting materials. ($Cr_{0.2}$,$Hf_{0.2}$,$Ta_{0.2}$,$Ti_{0.2}$,$Zr_{0.2}$)B_2 (HEB-Cr) and ($Hf_{0.2}$,$Nb_{0.2}$,$Ta_{0.2}$,$Ti_{0.2}$,$Zr_{0.2}$)C (HEB-Nb) were the target compositions for the HEB and HEC with synthesis by boro/carbothermal reduction (BCTR) of oxides. The formation reactions for the constituent phases are shown in Reaction (1) for the HEB and Reaction (2) for the HEC [15,16]:

$$0.4\ HfO_2+0.4\ ZrO_2+0.4\ TiO_2+0.2\ Ta_2O_5+0.2\ Cr_2O_3+B_4C+3C=2(Cr_{0.2},Hf_{0.2},Ta_{0.2},Ti_{0.2},Zr_{0.2})B_2+4\ CO \quad (1)$$

$$0.2\ HfO_2+0.2\ ZrO_2+0.2\ TiO_2+0.1\ Ta_2O_5+0.1Nb_2O_5+3.2C=(Hf_{0.2},Nb_{0.2},Ta_{0.2},Ti_{0.2},Zr_{0.2})C+2.2\ CO \quad (2)$$

Oxides, carbon, and B_4C were batched in proportions to produce 85 wt% HEB and 15 wt% HEC. Excess B_4C is typically added to Reaction (1) to compensate for loss of B due to evaporation of boron oxide species during HEB synthesis. However, in this study, the stoichiometric amount of B_4C was used to avoid consuming the HEC phase by reaction with excess B_4C according to Reaction (3) [14].

$$2HEC+B_4C\rightarrow HEB+3C \quad (3)$$

The oxides and stoichiometric amounts of B_4C and carbon were mixed by conventional ball milling at 70 rpm for 4 h using yttria-stabilized ZrO_2 media and acetone. Then, the slurries were dried at 65 °C using rotary evaporation (Model Rotavapor R-124: Buchi, Flawil, Germany). The dried powders were passed through a 60-mesh sieve. To improve particle contact, promote reactions, and suppress loss of powder during processing, powder mixtures were compacted into disks with a diameter of 60 mm using a uniaxial pressure of 2 MPa. Synthesis of dual-phase HEB-HEC powders by BCTR was performed at 1650 °C for 3 h in a resistance-heated graphite element furnace (Model HP50–7010 G, Thermal Technology, Santa Rosa, CA) under mild vacuum (~3 Pa) [17]. Products were crushed and passed through a 100-mesh metallic sieve. The reacted powder mixtures were further ball milled for 24 h using WC media in acetone to promote homogeneous intermixing of formed borides and carbides and solid solution for the subsequent densification process.

Reacted and ball milled powder mixtures were densified by a two-step SPS (DCS10, Thermal Technology) process [17]. The first stage was heating at 100 °C/min under mild vacuum (~2 Pa) at a uniaxial load of 15 MPa to 1650 °C where the temperature was held for 5 min to promote reaction and removal of residual oxides. In the second stage, the uniaxial pressure was increased to 50 MPa after holding at 1650 °C. The furnace was then heated at 150 °C/min to the final densification temperature, which ranged from 1900 to 1950 °C. After isothermal holding at the final temperature for 10 min, the furnace was cooled to 1000 °C at 50 °C/min and under a uniaxial pressure of 25 MPa and then cooled at the natural furnace rate to room temperature. The temperature was measured by an optical pyrometer focused on a hole that was drilled to a depth corresponding to half the thickness of the graphite die body.

Phase compositions were analyzed by x-ray diffraction (XRD, PANalytical X-Pert Pro, Malvern Panalytical Ltd., Royston, United Kingdom). Sintered specimens were ground on both sides to remove the graphite foil and any reaction layers. Oxygen contents were measured by inert gas fusion method (TS500 LECO, St. Joseph, MI). Bulk densities were measured by Archimedes' method using distilled water as the immersing medium. Theoretical densities were estimated from the metal ratios measured by energy-dispersive spectroscopy (EDS) and the measured lattice parameters determined by analyzing XRD patterns using Rietveld refinement (RIQAS software, MDI, Livermore, CA). Microstructures, grain sizes, chemical compositions, and distributions of metals were examined using a scanning electron microscope (SEM, Raith eLine Plus, Dortmund, Germany) equipped with energy-dispersive spectroscopy (EDS, Quantax Bruker, Billerica, MA). Specimen surfaces were polished to a 0.25 μm finish using successively finer diamond suspensions. Grain sizes were estimated by analyzing SEM images using computerized image analysis program (ImageJ, National Institutes of Health, Bethesda, MD) of at least 500 grains per specimen.

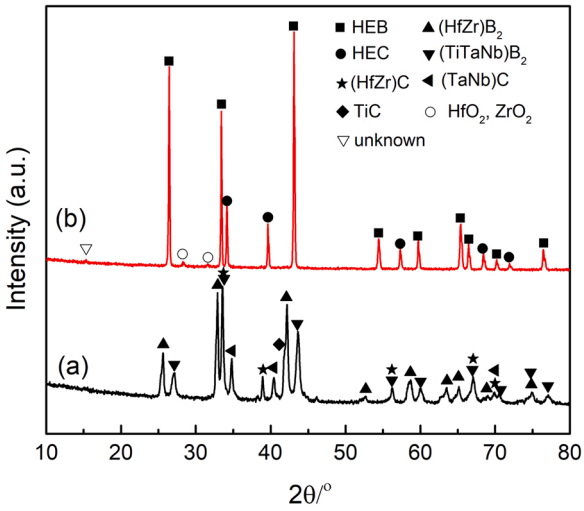

Fig. 1. XRD patterns of (a) the synthesized powder mixtures after BCTR at 1650 °C and (b) the dual-phase HEB-HEC ceramics after SPS at 1950 °C.

Microhardness was measured by Vickers indentation following ASTM C1327 (Duramin 5, Struers Inc., Cleveland, OH), under indentation loads of 0.49 N, 0.98 N, 1.96 N, 4.90 N, and 9.81 N for a dwell time of 15 s. Reported values are the average of 10 valid measurements. To minimize the error for testing a load of less than 4.90 N, indentation sizes were measured using a 3D digital optical microscope (HiROX, HIROX-USA, Hackensack, NJ).

3. Results and discussion

XRD patterns of the synthesized powder mixtures indicated that nominally pure boride and carbide mixtures were obtained after BCTR at 1650 °C, as shown in Fig. 1(a). In addition, oxides were not detected by XRD in the synthesized powder mixtures. The oxygen content was 0.56 wt%. The results indicated that the BCTR and CTR reactions were complete at 1650 °C, even though solid solution was not complete due to the low synthesis temperature. Similar to the previous studies [16,17], two distinct boride phases with the same hexagonal structure, but different lattice parameters, were observed in the XRD patterns for the powders synthesized at 1650 °C. One was nominally a HEB phase containing all five TMs, while the other one was nominally (Hf,Zr)B_2 due to the larger lattice parameters of HfB_2 and ZrB_2. In contrast, the powder contained at least four carbide phases, which included HEC, (Hf,Zr)C, (Ta,Nb)C, and TiC.

After densification at 1950 °C by SPS, XRD detected two distinct phases plus a trace amount of oxide that appeared to be HfO_2, ZrO_2, or both. One of the main phases had a hexagonal AlB_2 structure and the

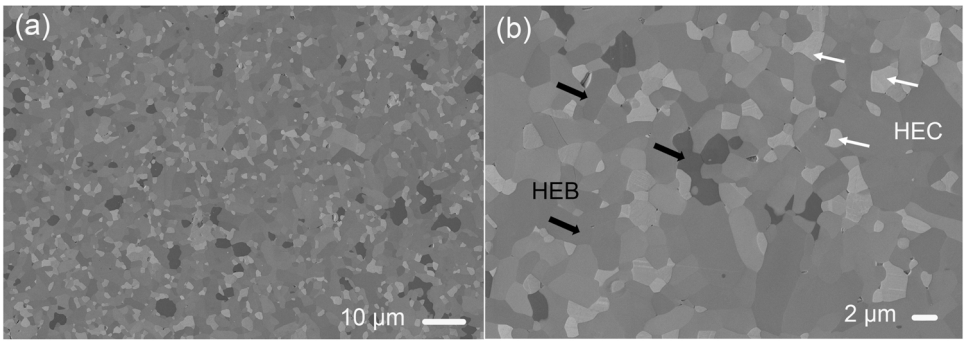

Fig. 2. Microstructures with (a) low and (b) high magnification for the dual-phase HEB-HEC ceramics. (The HEB phase has medium or dark contrast and is continuous while the HEC phase is lighter and isolated).

other one had a cubic rock salt structure as shown in Fig. 1(b). The results were consistent with XRD patterns for HEB and HEC phases from previous studies [8,17]. Comparing to the results of the synthesized powder mixtures, the formation of single HEB and HEC phases indicated that solid solutions the metals into the HEB and HEC phases reached completion during densification. A composition of 89.4 wt% HEB and 10.6 wt% HEC was estimated for the final ceramics by Rietveld refinement of XRD patterns. This composition had a lower HEC content than the designed composition, which could be due to the following reasons: 1) errors in the refinement because of the unknown elemental distributions between the HEB and HEC; or 2) HEC consumption during synthesis or densification by Reaction (3).

Other studies have typically required high-energy ball milling to produce single-phase HEB or HEC ceramics based on the need to reduce the particle size of the starting powders to improve intermixing of each component [7–17]. However, the present study demonstrated an easier process to produce the nominally pure HEB and HEC ceramics by BCTR using only conventional ball milling (i.e., 70 rpm rotation) followed densification. The homogeneity of the synthesized borides and carbides after BCTR was improved by adding an additional ball milling step after the BCTR process, thus resulting in the formation of nominally pure HEB and HEC after SPS. The oxygen content of powder mixtures was not significantly increased after the additional milling (0.56 wt% after synthesis vs 0.82 wt% after ball milling), while only 0.1 wt% contamination was introduced from WC media. This contamination might contribute to the unknown phase that was observed in XRD data. In contrast, without the additional milling step after BCTR, the solid solution was not complete after SPS (Figs. S1 and S2).

Fully dense and fine microstructures with homogeneously distributed HEB (darker) and HEC (lighter) phases were observed in the ceramics after SPS, as shown in Fig. 2. The phase with lighter contrast was the HEC phase based on EDS data. The amount of HEC was determined to be ~14.5 wt% by Rietveld refinement of XRD data (~14.5 wt%). The different levels of contrast among HEB grains was due to channeling contrast differences that results from the orientation of the grains. This effect is commonly reported for SEM of electrically conductive boride and carbide ceramics when specimens are examined at low accelerating voltages without a conductive coating [18,19]. The average grain sizes were 2.7 ± 1.3 μm for the HEB and 1.6 ± 0.7 μm for the HEC. Similar grain sizes of 1.1 ± 0.4 μm for the HEB (23 vol%) and 1.2 ± 0.4 μm for the HEC (77 vol%) in a dual-phase (Hf,Nb,Ta,Ti,W,Zr)B_2-(Hf,Nb,Ta,Ti,W,Zr)C reported by Smith et. al [14]. Similarly, Luo et al. [13] reported average grain sizes of 0.6–2.6 μm for the HEB and 0.5–2.3 μm for the HEC in dual-phase ceramics containing (Hf,Nb,Ta,Ti,Zr)B_2 and different contents of (Hf,Nb,Ta,Ti,Zr)C. Qin et al. [11] reported average grain sizes of 4–15 μm for the HEB and 5–12 μm for the HEC in their dual-phase HEB-HEC ceramic. The difference in the average grain sizes between current and previous studies was due to the different compositions, starting materials, and processing methods. The bulk density of dual-phase ceramic was 8.35 g/cm^3. Area analysis of the SEM images showed a composition of 85.5 wt% HEB and 14.5 wt% HEC with a negligible amount of porosity, which was consistent with the designed composition. The area analysis seems more precise than the XRD refinement due to the more precise measurement of the distribution of phases that is possible in the SEM images.

Chemical composition analysis was used to determine the TM contents in the HEB and HEC phases. Elemental distributions for Cr, Hf, Nb, Ti, Ta, and Zr are shown in Fig. 3. Hf and Ta appeared to segregate preferentially to the carbide phase, while Ti, Nb, Zr, and Cr had higher contents in the boride phase. The preferential solid solution in the HEB and HEC phases could depend on the different formation energies of HEB and HEC phases with different metal ratios [11]. The preferential segregation of the heavier metals (i.e., Ta and Hf) to the minor carbide phase made their contents appear higher than the formulated amounts.

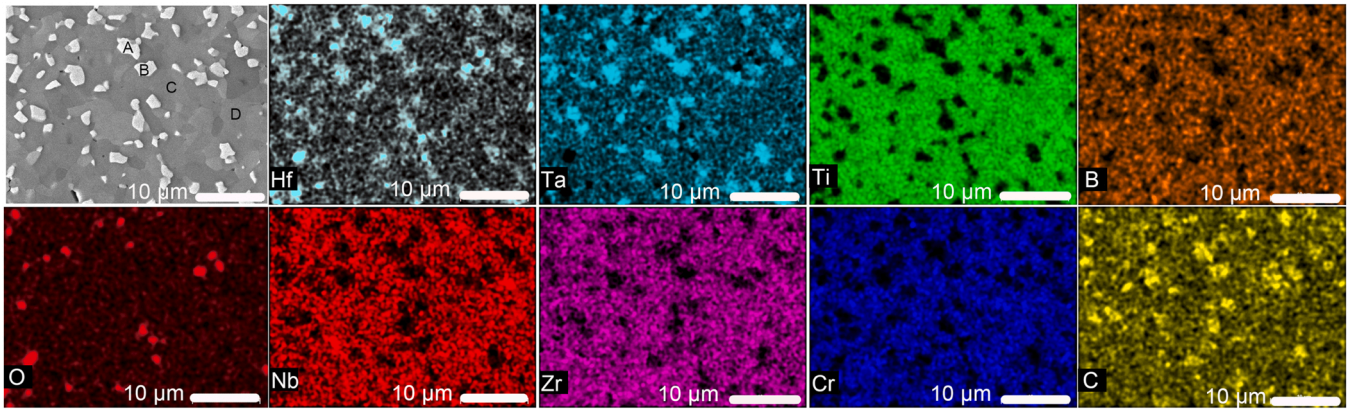

Fig. 3. Microstructure and corresponding EDS maps of the dual-phase HEB-HEC ceramics. In the SEM image, the HEC is the phase with lighter contrast.

Table 1
Atomic compositions of the HEC and HEB from EDS.

Phase/Points		Metal elements (at%) Hf	Zr	Ti	Ta	Nb	Cr	Density (g/cm^3)
HEC	A	29.7	24.9	7.5	35.5	1.3	1.1	11.13
	B	27.5	24.6	8.5	36.6	1.4	1.4	
HEB	C	16.3	27.8	24.9	19.2	3.9	7.9	7.81
	D	17.6	28.1	23.6	18.2	4.3	8.2	

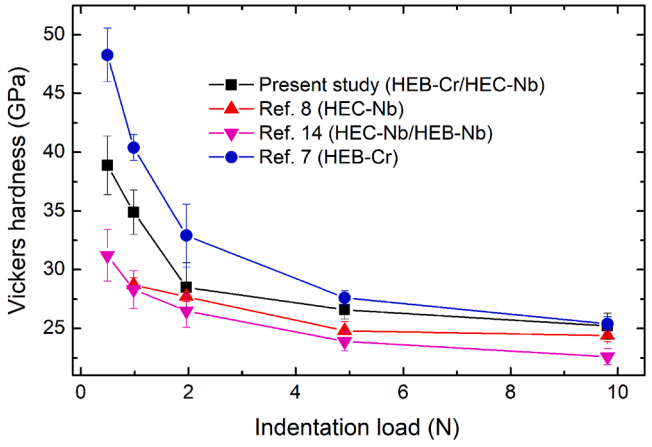

Fig. 4. Vickers hardness as a function of load.

The ratios of Cr and Nb that preferentially segregated to the major phase appeared lower than the batched amounts due to the different amounts of HEB and HEC in the final ceramic. A trace amount (less than 1 wt%) of oxygen was detected by EDS, which was consistent with XRD data that also detected trace amounts of an oxide phase. Based on the EDS analysis on each phase, summarized in Table 1, the nominal composition of HEB is approximately $(Cr_{0.08},Hf_{0.17},Nb_{0.04},Ta_{0.19},Ti_{0.24},Zr_{0.28})B_2$ and the HEC is $(Cr_{0.01},Hf_{0.29},Nb_{0.01},Ta_{0.36},Ti_{0.08},Zr_{0.25})C$. Compared to previous studies, W contamination was minimized by avoiding high-energy ball milling using WC media in the present study [11,14].

Vickers hardness values of the dual phase HEB-HEC ceramics as a function of indentation load are compared to values from previous studies in Fig. 4. The hardness values of the dual phase HEB-HEC ceramic increased from 25.2 ± 1.1 to 38.9 ± 2.5 GPa as the indentation load decreased from 9.81 to 0.49 N. The values were between values for the desired constituents, which were HEB-Cr and HEC-Nb. The previous study reported that HEB-Cr had the highest Vickers hardness, at 48.3 ± 2.3 GPa, among the current reported HEB ceramics. Therefore, dual phase HEB-HEC ceramics produced in the present study had higher hardness values at 1.96 N than dual phase HEB-HEC ceramics reported in previous studies (26.5 ± 1.4 GPa [14], 21 GPa~27 GPa [13], 21–25 GPa [11]) due to the hardening effect of Cr and the higher relative density of the ceramics in the present study. Even though preferential segregation of transition metals to either the HEB or HEC was observed, and the target compositions were not reached, the hardness values of the dual phase ceramics produced followed a rule of mixtures from values reported for the desired constituent HEB and HEC phases. Although no synergistic hardening was observed for the specific dual-phase ceramics beyond what was already obtained in the single phase HEB and HEC constituents, further synergistic hardening may be possible for different HEB:HEC ratios, transition metal constituents, or microstructures.

4. Conclusions

Dense, dual-phase high-entropy boride-carbide ceramics were produced by spark plasma sintering of powders synthesized by boro/carbothermal reduction of oxides. The compositions of the constituent phases were found to be approximately $(Cr_{0.08},Hf_{0.17},Nb_{0.04},Ta_{0.19},Ti_{0.24},Zr_{0.28})B_2$ and $(Cr_{0.01},Hf_{0.29},Nb_{0.01},Ta_{0.36},Ti_{0.08},Zr_{0.25})C$. The high-entropy carbide content of the final ceramics was about 14.5 wt%. The average grain sizes were 2.7 ± 1.3 μm for the high-entropy boride phase and 1.6 ± 0.7 μm for the high-entropy carbide phase, due to the pinning effect and the boro/carbothermal reduction process. Hf and Ta segregated preferentially to the carbide phase, while Ti, Nb, Zr, and Cr showed higher contents in the boride phase, which was presumably due to the different formation energies of HEB and HEC phases with different metal ratios. The Vickers hardness values increased from 25.2 ± 1.1 to 38.9 ± 2.5 GPa as the indentation load decreased from 9.8 to 0.49 N. This study demonstrated a simplified process for synthesizing dual-phase HEB-HEC ceramics that utilized conventional ball milling, which resulted in lower contents of oxygen and tungsten impurities than processes that utilize high energy ball milling while still forming phase-pure ceramics with nearly full density.

Declaration of Competing Interest

The authors declare that they have no known competing financial interests or personal relationships that could have appeared to influence the work reported in this paper.

Acknowledgments

The authors thank Dr. Xiomara Campilongo for fruitful discussions. Funding for this research was provided by the Office of Naval Research through a Multidisciplinary University Research Initiative (MURI) program under project number N00014-21-1-2515.

Appendix A. Supplementary material

Supplementary data associated with this article can be found in the online version at doi:10.1016/j.jeurceramsoc.2022.12.056.

References

[1] C. Oses, C. Toher, S. Curtarolo, High entropy ceramics, Nat. Rev. Mater. 5 (2020) 295–309.
[2] L. Feng, W.G. Fahrenholtz, D.W. Brenner, High-entropy ultra-high-temperature borides and carbides: a new class of materials for extreme environments, Annu. Rev. Mater. Res. 51 (2021) 165–185.
[3] L. Feng, W.T. Chen, W.G. Fahrenholtz, G.E. Hilmas, Strength of single-phase high-entropy carbide ceramics up to 2300ºC, J. Am. Ceram. Soc. 104 (2021) 419–427.
[4] L. Backman, J. Gild, J. Luo, E.J. Opila, Part II: experimental verification of computationally predicted preferential oxidation of refractory high entropy ultra-high temperature ceramics, Acta Mater. 197 (2020) 81–90.
[5] J. Gild, Y.Y. Zhang, T.J. Harrington, S.C. Jiang, T. Hu, M.C. Quinn, W.M. Mellor, N. X. Zhou, K.H. Vecchio, J. Luo, High-entropy metal diborides: a new class of high entropy materials and a new type of ultrahigh temperature ceramics, Sci. Rep. 6 (2016) 37946.
[6] P. Sarker, T.J. Harrington, C. Toher, C. Oses, M. Samiee, J.P. Maria, D.W. Brenner, K.S. Vecchio, S. Curtarolo, High-entropy high-hardness metal carbides discovered by entropy descriptors, Nat. Commun. 9 (2018) 4980.
[7] L. Feng, F. Monteverde, W.G. Fahrenholtz, G.E. Hilmas, Superhard high-entropy AlB_2-type diboride ceramics, Scr. Mater. 199 (2021), 113855.
[8] L. Feng, W.G. Fahrenholtz, G.E. Hilmas, Low-temperature sintering of single-phase, high-entropy carbide ceramics, J. Am. Ceram. Soc. 102 (2019) 7217–7224.
[9] B.L. Ye, T.Q. Wen, K.H. Huang, C.Z. Wang, Y.H. Chu, First-principles study, fabrication, and characterization of (Hf0.2Zr0.2Ta0.2Nb0.2Ti0.2)C high-entropy ceramic, J. Am. Ceram. Soc. 102 (2019) 4344–4352.
[10] X.L. Yan, L. Contantin, Y.F. Lu, J.F. Silvain, M. Nastasi, B. Cui, $(Hf_{0.2}Zr_{0.2}Ta_{0.2}Nb_{0.2}Ti_{0.2})C$ high-entropy ceramics with low thermal conductivity, J. Am. Ceram. Soc. 101 (2018) 4486–4491.
[11] M. Qin, J. Gild, C.Z. Hu, H.R. Wang, M.S.B. Hoque, J.L. Braun, T.J. Harrington, P. E. Hopkins, K.S. Vecchio, J. Luo, Dual-phase high-entropy ultra-high temperature ceramics, J. Eur. Ceram. Soc. 40 (2020) 5037–5050.
[12] S.J. Huo, L. Chen, X.R. Liu, Q.Y. Kong, Y.J. Wang, H. Gu, Y. Zhou, Reactive sintering of dual-phase high-entropy ceramics with superior mechanical properties, J. Mater. Sci. Technol. 129 (2022) 223–227.
[13] S.C. Luo, W.M. Guo, K. Plucknett, H.T. Lin, Fine-grained dual-phase high-entropy ceramics derived from boro/carbothermal reduction, J. Eur. Ceram. Soc. 41 (2021) 3189–3195.

[14] S.M. Smith II, L. Feng, W.G. Fahrenholtz, G.E. Hilmas, T.S. Huang, High-entropy boride-carbide ceramic by sequential boro/carbothermal reaction, J. Am. Ceram. Soc. 105 (2022) 5543–5547.
[15] L. Feng, W.G. Fahrenholtz, G.E. Hilmas, Y. Zhou, Synthesis of single-phase high-entropy carbide powders, Scr. Mater. 162 (2019) 90–93.
[16] L. Feng, W.G. Fahrenholtz, G.E. Hilmas, Two-step synthesis process for high-entropy diboride powders, J. Am. Ceram. Soc. 103 (2020) 724–730.
[17] L. Feng, W.G. Fahrenholtz, G.E. Hilmas, Processing of dense high-entropy boride ceramics, J. Eur. Ceram. Soc. 40 (2020) 3815–3823.
[18] D. Sciti, S. Guicciardi, M. Nygren, Densification and mechanical behavior of HfC and HfB2 fabricated by spark plasma sintering, J. Am. Ceram. Soc. 91 (2008) 1433–1440.
[19] E.W. Neuman, G.E. Hilmas, W.G. Fahrenholtz, Processing, microstructure, and mechanical properties of large-grained zirconium diboride ceramics, Mater. Sci. Eng. A 670 (2016) 196–204.